RUSSIAN JOURNAL OF EARTH SCIENCES
vol. 19, 5, 2019, doi: 10.2205/2019ES000679

# Thermohaline structure of Antarctic Bottom Water in the abyssal basins of the South Atlantic

*D. I. Frey*[1], *E. G. Morozov*[1], *I. Ansorge*[2], *V. V. Fomin*[3], *N. A. Diansky*[3,4,5], *R. Yu. Tarakanov*[1]

[1]Shirshov Institute of Oceanology RAS, Moscow, Russia

[2]University of Cape Town, Rondebosch, South Africa

[3]Zubov State Oceanographic Institute, Moscow, Russia

[4]Lomonosov Moscow State University, Moscow, Russia

[5]Institute of Numerical Mathematics RAS, Moscow, Russia

**Abstract.** Antarctic Bottom Water (AABW) occupies the lowest ocean layer in the major part of the Atlantic. Despite the fact that this water has the same origin from the Weddell Sea, thermohaline properties of bottom layers vary strongly in different deep basins. Temperature and salinity increase along the pathways of bottom water propagation is caused by mixing of AABW with the warmer and more saline water in the overlying layers. This mixing strongly intensifies over underwater ridges; in addition, these ridges determine the pathways of bottom water spreading. Thus, the ocean topography plays the most important role in the formation of thermohaline structure of deep basins. In particular, the properties of AABW in the western and eastern parts of the South Atlantic significantly differ from each other. In this paper we compare temperature and salinity structure of the abyssal waters of the

This is the e-book version of the article, published in Russian Journal of Earth Sciences (doi:10.2205/2019ES000679). It is generated from the original source file using LaTeX's **ebook.cls** class.

Southeast and Southwest Atlantic. We used the results of high spatial resolution modeling and hydrographic measurements for this study. We also simulated the velocity field in the bottom layer of the South Atlantic.

## The Data and Methods

Sparse direct observations in the abyssal ocean layer make investigations of bottom waters structure difficult. Simulations with modern numerical models focus on the calculation in the upper part of the ocean; usually, vertical resolution of these models in the deep layers is not sufficient for describing abyssal processes. In this work, we combined two approaches: first of all, we simulated the deep-water circulation using a regional model with a high resolution in the deep layers; in addition, we used direct hydrographic measurements for verification of the model and for detailed analysis of AABW evolution along the pathways of its spreading.

The Institute of Numerical Mathematics Ocean Model (INMOM) [*Zalesny et al.,* 2010] was used for the simulations. The INMOM is a $\sigma$-coordinate numerical model based on the primitive equations of hydrothermodynamics with the Boussinesq and hydrostatic approximations [*Diansky et al.,* 2002; *Frey et al.,* 2017a, 2017b; *Morozov et al.,* 2019; *Zalesny et al.,* 2012]. The model domain covered the part of the Atlantic Ocean from the equator to 50°S, and from 60°W to 20°E (the domain is shown with thick black lines in Figure 1). The horizontal resolution was 0.05° by latitude and longitude, which gives $1600 \times 1000$ model points in the horizontal plane. The domain covers the deep basins of the West and East Atlantic: Angola, Cape, Argentine, and Brazil basins are the regions, which we want to investigate and compare in this study.

The bottom relief was interpolated to the model domain from the GEBCO 2014 digital database [*Weatherall et al.,* 2015]. The climatological data from the World Ocean Atlas 2013 [*Locarnini et al.,* 2013; *Zweng et al.,* 2013] were used as the initial temperature and salinity fields. These data were also specified in a buffer zone with a width of 10 grid points at the liquid boundaries [*Klinck,* 1995]. The atmosphere-ocean interaction was prescribed by specifying the fluxes of heat, freshwater, and momentum at the boundary. The atmospheric characteristics included air temperature, humidity, and wind velocity at a height of 10 m, atmospheric pressure, longwave and shortwave irradiance, and monthly mean precipitation. They were taken from the CORE database [*Large and Yeager,* 2009]. The numerical experiment was performed in two stages: at first, the model was spun up using "frozen" temperature and salinity fields; then, the simulation included adjustment of thermohaline properties. This method was suggested in [*Sarkisyan,* 1991] for computing the velocity field based on known temperature and salinity data.

Prognostic variables of the model are three-dimensional fields of potential temperature, salinity, and components of horizontal velocity. Here, we analyzed temperature and salinity fields on the last day of the calculation. We used the data from two quasi-meridional hydrographic sections (the locations of stations over these sections are indicated with white dots in Figure 1). We chose these two sections because they follow the deep part of the basins in the West and East Atlantic and represent transformation of AABW properties. The first section across the Argentine and Brazil basins was occupied during cruise 17 of the R/V *"Akademik Sergei Vavilov"* in 2003 [*Morozov,* 2005]. The route of this cruise covered the main pathway of Antarctic Bottom Water spreading. The data acquisition system consisted of a General Oceanics Rosette multi-bottle array system and Neil Brown CTD profiler. The second section across the eastern basins was carried out during the cruise of the R/V *"Ronald H. Brown"* along line A13.5 [*Bullister et al.,* 2010]. The data were collected using Sea-Bird Electronics (SBE) 9plus CTD profiler mounted in a SBE 32 aluminum frame.

# Model Verification and Meridional Evolution of AABW Properties

The results of numerical modeling were compared with the direct measurements over two sections in the West and East Atlantic (Figure 1) because bottom water structures in these two regions differ significantly. Quasi-meridional direction of these sections allows us to verify how the model reproduces the evolution of AABW properties. Moreover, the locations of stations in cruise 17 of the R/V *"Akademik Sergei Vavilov"* were especially chosen along the main pathway of AABW spreading. These stations include the Vema Channel with the most intense flow of AABW in the Atlantic. In the channel, CTD casts were performed near its eastern wall [*Morozov,* 2005], because the Ekman friction moves the coldest waters to the right relatively to the main northward flow (in the Southern Hemisphere).

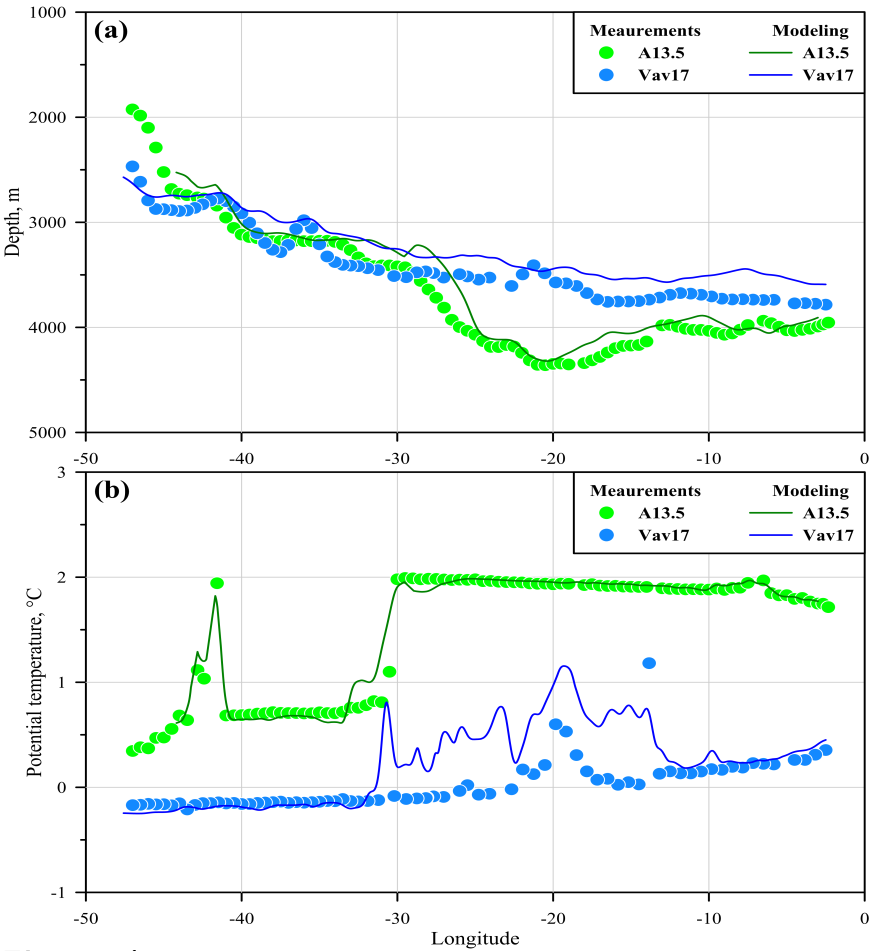


**Figure 1.** The data used for verification of the model: depth of 2°C potential temperature isotherm (a) and potential temperature at the ocean bottom (b) along the hydrographic sections in the West (shown with blue colors) and East (green colors) Atlantic. Circles indicate the values at the CTD-stations; solid lines are the data of numerical modeling interpolated to the trajectory of the sections. Some statistical parameters of these data are given in Table 1.

**Table 1.** Verification of the Model on the Basis of Two CTD-Sections. $X_{model}$ and $X_{meas}$ are Modeled and Measured Values, Respectively. These Values Include Calculated Upper Boundary of AABW and Potential Temperature at the Ocean Bottom

| | Maximum $(X_{model} - X_{meas})$ | Minimum $(X_{model} - X_{meas})$ | Mean $(X_{model} - X_{meas})$ | Standard deviation $(X_{model} - X_{meas})$ |
|---|---|---|---|---|
| AABW level (East), m | 103 | −402 | −117 | 109 |
| AABW level (West), m | 217 | −303 | −159 | 101 |
| Bottom pot. temp. (East), °C | 0.55 | −0.20 | 0.018 | 0.110 |
| Bottom pot. temp. (West), °C | 0.66 | −0.85 | 0.092 | 0.401 |

This effect was investigated in the Vema Channel numerically [*Jungclaus and Vanicek,* 1999] and observed many times in different expeditions [*Morozov et al.,* 2008, 2010]. The flow of AABW from the Vema Channel was studied in [*Morozov et al.,* 2018].

The data used for verification are shown in Figure 2. We compared two properties of AABW: the depth of its upper boundary (Figure 2a), and potential temperature at the ocean bottom (Figure 2b). The stations occupied in cruise 17 of the R/V *"Akademik Sergei Vavilov* are shown with blue color, and stations from the A13.5 section occupied in the cruise of the R/V *"Ronald H. Brown"* are shown with green. Solid lines in Figure 2 correspond to the results of our numerical modeling. Bottom temperatures were determined as the temperature of the closest to the bottom sample; usually the CTD cast was stopped at 3–5 meters above the sea floor. As for numerical modeling, potential temperature from the lowest sigma-level was used for comparison with the measured value. The location of the 2$^\circ$C isotherm at the station was determined by linear interpolation of the temperature profile between samples; the same approach was used for simulated data.

The simulated data presented in Figure 2 were in-

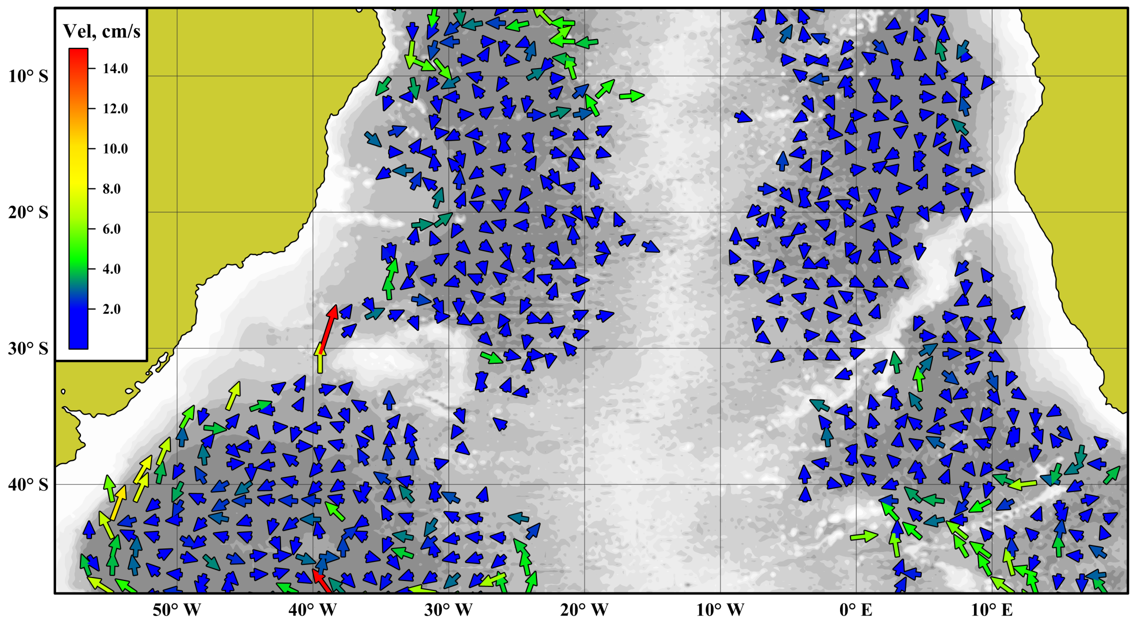


**Figure 2.** Vectors of horizontal velocities at a depth of a 4300 m in the South Atlantic based on the results of numerical modeling.

terpolated to the points of measurements for model verification. Parameters of data comparison are shown in Table 1. Standard deviation of the difference between simulated and measured values is about 100 meters over both sections. Simulated bottom potential temperatures over the A13.5 section agree well with the measurements (the mean difference is 0.018°C and standard deviation is 0.11°C). As can be seen from Figure 2b, the temperatures in the West Atlantic at latitudes of 32°–15°S differ significantly. One of the causes of this discrepancy is the narrowness of the Vema Channel located at this part of the section. The resolution of the model does not allow one to restore the AABW flow adequately; thus, simulated values do not agree with the correctly measured ones. The correct simulation is presented in [*Frey et al.,* 2017a] using the same model with much higher horizontal resolution.

## AABW Structure and Velocities in the Bottom Layer of the Atlantic

The results of numerical modeling allow us to study the spatial structure of bottom waters in the South Atlantic. For this analysis, we interpolated three-dimensi-

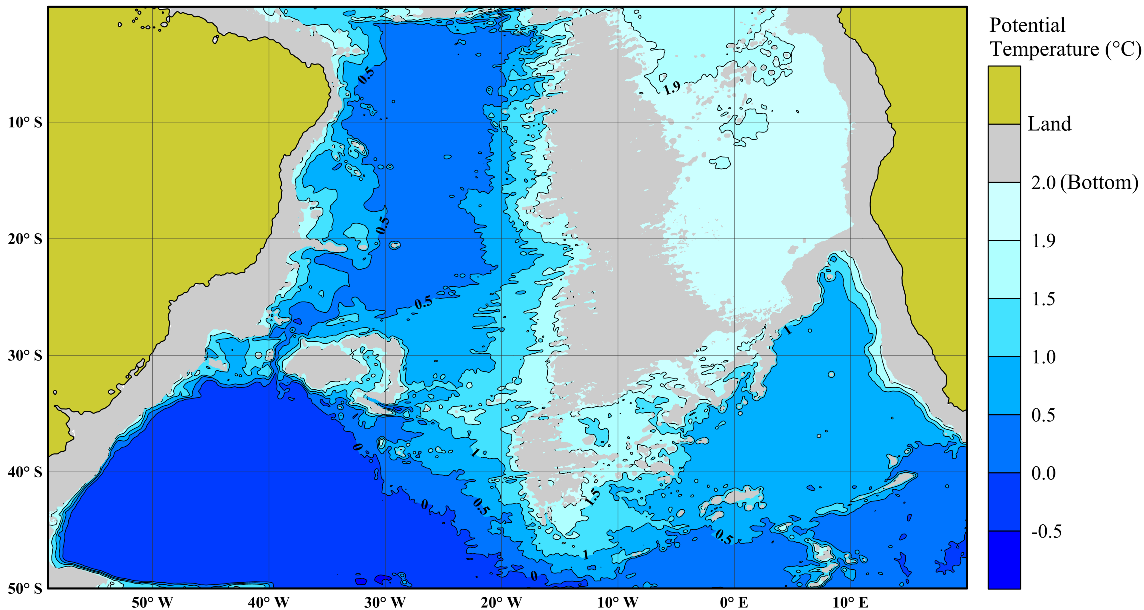


**Figure 3.** Bottom potential temperature in the bottom layer of the Atlantic. The data were taken from the deepest $\sigma$-level of the model. The ocean basins with bottom potential temperature greater than 2°C are shown with gray color.

onal temperature and salinity fields from vertical sigma-levels to regular $z$-levels with high resolution. Using interpolated data, we calculated horizontal velocities in the AABW layer in the entire South Atlantic (Figure 3). Here we present the velocities at a depth of 4300 m, which corresponds to a depth of the main flow in the Vema Channel. Generally, these velocities do not exceed 5 cm/s; more intense flows are observed in the western part of the Argentine Basin and in the Vema Channel. Correct modeling of these flows requires higher resolution. The main feature of the bottom circulation in the western part of the South Atlantic is the bottom flow of the Deep Western Boundary Current directed to the north. This current is clearly pronounced south of the Rio Grande Rise (south of 30°S). Strong intensification of the bottom current occurs in the Vema Channel (27°–33°S). Based on the numerical modeling, the northerly current becomes less intense north of 27°S and almost disappears in the northern part of the Brazil Basin. However, direct measurements in the ocean reveal that the northerly bottom flow continues further to the equator and north of the equator [*Sandoval and Weatherly,* 2001].

In the East Atlantic, the inflow of AABW to the Angola Basin based on numerical simulations is revealed in the southern part of the Angola Basin. This conclusion was also made in [*Morozov et al.,* 2010]. The circulation in the bottom layer of the Angola Basin is generally very weak.

Some aspects of deep-water circulation in this region are discussed in [*Frey et al.,* 2017b]. Distribution of bottom potential temperature (Figure 4) is helpful for determining the main pathways of AABW spreading. The values of potential temperature were taken from the bottom $\sigma$-level of our model.

We calculated some integral parameters of AABW in the main basins of the South Atlantic. The parameters include minimum potential temperature and salinity, maximum potential density referenced to 4000 db ($\sigma_4$), and total volume of Antarctic waters below the 2°C potential temperature isotherm (Table 2). The calculation was made for the Argentine, Brazil, Cape, and Angola basins separately. Minimum temperatures were determined from the deepest sigma-level of the model. Usually, the waters with the minimum temperatures are located in the deep part of the basins near the channel with inflow of bottom waters. The minimum salinity in Table 2 was determined as salinity at the points with minimum temperature. Then, maximum potential density referenced to 4000 db was

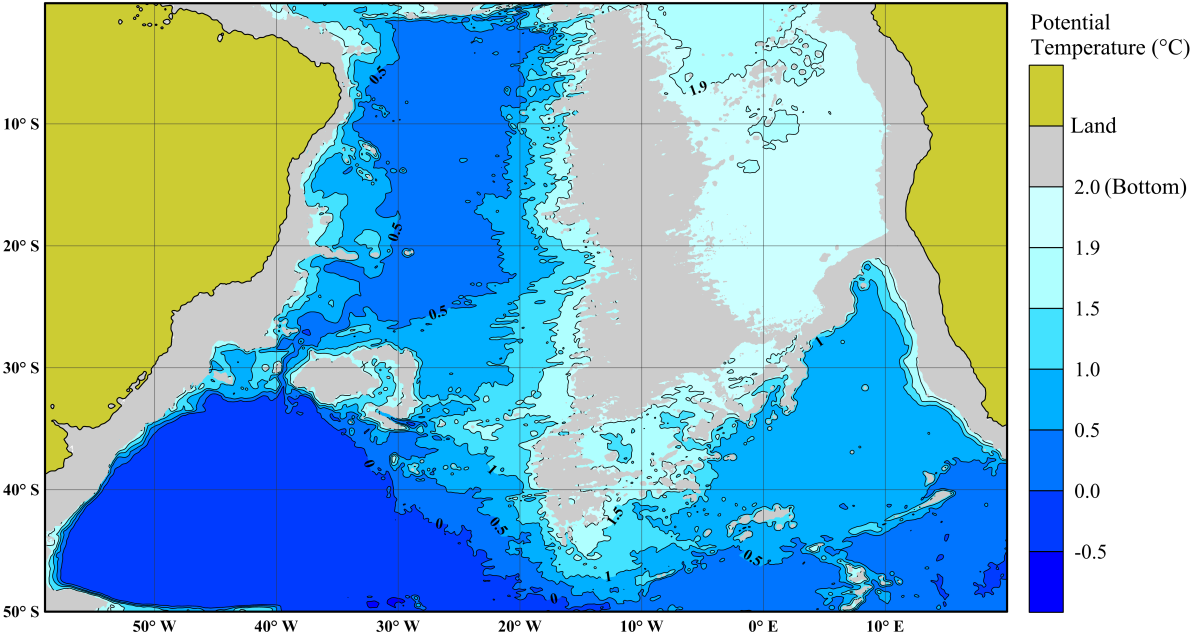


**Figure 4.** Bottom potential temperature in the bottom layer of the Atlantic. The data were taken from the deepest $\sigma$-level of the model. The ocean basins with bottom potential temperature greater than 2°C are shown with gray color.

derived using the EOS80 equations [*Lewis and Perkin,* 1981]. Three-dimensional temperature field interpolated to the $z$-levels was used for the calculation of the AABW volume. Horizontal resolution of the field was $0.05^\circ$ (the same as the model resolution), the vertical resolution was 20 meters. Then, we made the following check for each point of the grid: if potential temperature $\theta$ was lower than $2^\circ$C and location of the node was above the bottom, then this volume was added to the corresponding ocean basin. We can see that the AABW volume in the West Atlantic is two times larger than in the East Atlantic; in addition, the waters west of the Mid-Atlantic Ridge are colder and less saline, which makes their density higher (Table 2).

## Summary and Conclusions

Temperature and salinity structure of bottom waters in deep basins of the South Atlantic were studied on the basis of two hydrographic quasi-meridional sections and simulations using a numerical model with a high resolution in the abyssal ocean layer. The model was verified using the CTD data from these sections. In this study, we focused on the transformation of bottom waters over the pathway of their propagation and

**Table 2.** AABW Properties in Deep Basins of the South Atlantic Based on the Numerical Simulation

| Basin | Minimum pot. temperature, °C | Minimum salinity, psu | Maximum density $\sigma_4$, kg/m$^3$ | Total AABW volume, $10^6$ km$^3$ |
|---|---|---|---|---|
| Argentine | −0.25 | 34.67 | 46.09 | 10.8 |
| Brazil | 0.15 | 34.69 | 46.05 | 9.2 |
| Cape | 0.6 | 34.71 | 45.99 | 5.6 |
| Angola | 1.9 | 34.88 | 45.88 | 3.5 |

on the zonal differences of AABW in the western and eastern parts of the South Atlantic Ocean. Some integral characteristics of bottom waters were calculated for the individual ocean basins, including the Argentine, Brazil, Cape, and Angola basins. The main results of our research related to the numerical simulations and model adjustment are as follows:

1. An adjusted version of the ocean circulation model was applied for investigations of the abyssal ocean layer, including the main pathways of bottom waters and influence of underwater ridges and other features of bottom topography on the spatial structure of deep waters. Narrow abyssal channels are key points of AABW propagation and require sufficient horizontal resolution of the model as well as additional verification.

2. Significant increase in the bottom temperature is observed over underwater ridges along the pathway of AABW propagation. In addition, its upper boundary becomes much deeper. For example, after crossing the ridge at 30°S in the Southeast Atlantic, the bottom potential temperature increases from 0.7°C up to 1.9°C, while the 2°C isotherm descends by almost 1 km.

3. Strong differences are observed in the abyssal waters in the Southwest and Southeast Atlantic due to the local peculiarities of the bottom topography. Thus, the total volume of AABW in the West Atlantic is two times greater than in the East Atlantic; the bottom temperature variations between them reach 2°C over the same zonal section.

4. The flow of AABW to the north is generally concentrated in the abyssal Deep Western Boundary Current. It is well pronounced in the Argentine Basin but becomes weaker in the Brazil Basin.

**Acknowledgments.** The work was carried out within the State Task of the Russian Federation 0128-2019-0009; the research was supported by the Russian Foundation for Basic Research (grant 19-57-60001, numerical simulations, and 19-05-00878, model adjustment) and by the Russian Science Foundation (grant 16-17-10149, data analysis). The work of I. Ansorge was supported by the National Research Foundation of South Africa (Grant UID 118901).

# References


Banyte, D., M. Morales Maqueda, R. Hobbs, D. A. Smeed, A. Megann, S. Recalde (2018) , Geothermal Heating in the Panama Basin: 1. Hydrography of the Basin, *J. Geophys. Res.*, *123*, no. 10, p. 7382–7392, **Crossref**

Bullister, J. L., R. A. Feely, R. Wanninkhoff, A. G. Dickson, D. A. Hansell, R. M. Key (2010) , *Carbon dioxide, hydrographic, and chemical data obtained during the R/V Ronald H. Brown Cruise in the Atlantic Ocean on CLIVAR repeat hydrography section A13.5 (Mar. 08–Apr. 17, 2010)*, Carbon Dioxide Information Analysis Center, Oak Ridge National Laboratory, U.S. Department of Energy, Oak Ridge, **Crossref**

De Lavergne, C., G. Madec, J. Le mmer, A. G. Nurser, A. C. Naveira Garabato (2016) , On the consumption of Antarctic Bottom Water in the abyssal ocean, *J. Phys. Oceanography*, *46*, no. 2, p. 635–661, **Crossref**

Diansky, N. A., A. V. Bagno, V. B. Zalesny (2002) , Sigma model of global ocean circulation and its sensitivity to variations in wind stress, *Izv. Atmosph. Oceanic Phys.*, *38*, no. 4, p. 537–556.

Dickson, R. R., J. Brown (1994) , The production of North Atlantic Deep Water: Sources, rates, and pathways, *J. Geophys. Res.*, *99*, p. 12,319–12,342, **Crossref**

Frey, D. I., V. V. Fomin, N. A. Diansky, et al. (2017a) , New model and field data on estimates of Antarctic Bottom Water flow through the deep Vema Channel, *Doklady Earth Sciences*, *474*, no. 1, p. 561–564, **Crossref**

Frey, D. I., A. N. Novigatsky, M. D. Kravchishina, E. G. Morozov (2017b) , Water structure and currents in the Bear Island Trough in July–August 2017, *Russ. J. Earth. Sci.*, *17*, p. ES3003, **Crossref**

Ganachaud, A., C. Wunsch (2000) , Improved estimates of global ocean circulation, heat transport and mixing from hydrographic data, *Nature*, *408*, p. 453–457, **Crossref**

Hogg, N., G. Siedler, W. Zenk (1999) , Circulation and variability at the Southern Boundary of the Brazil Basin, *J. Phys. Oceanogr.*, *29*, p. 145–157, **Crossref**

Johnson, G. C. (2008) , Quantifying Antarctic Bottom Water and North Atlantic Deep Water volumes, *J. Geophys. Res.*, *113*, p. C05027, **Crossref**

Jungclaus, J., M. Vanicek (1999) , Frictionally modified flow in a deep ocean channel: Application to the Vema Channel, *J. Geophys. Res.*, *104*, no. C9, p. 21,123–21,136, **Crossref**

Klinck, J. M. (1995) , Thermohaline structure of an eddy-resolving North-Atlantic model: The influence of boundary conditions, *J. Physical Oceanography*, *25*, p. 1174–1196, **Crossref**

Large, W., S. Yeager (2009) , The global climatology of an interannually varying air-sea flux data set, *Clim. Dyn.*, *33*, p. 341–364, **Crossref**

Lewis, E. L., R. G. Perkin (1981) , The Practical Salinity Scale 1978: conversion of existing data, *Deep-Sea Research*, *28A*, no. 4, p. 307–328, **Crossref**

Locarnini, R. A., A. V. Mishonov, J. I. Antonov, et al. (2013) , *World Ocean Atlas 2013, Vol. 1: Temperature, S. Levitus* *(ed.), A. Mishonov (techn. ed.)*, 40 pp., NOAA Atlas NESDIS 73, USA (http://www.nodc.noaa.gov/OC5/indprod.ht ml).

Lumpkin, R., K. Speer (2007) , Global ocean meridional overturning, *J. Physical Oceanography*, *37*, p. 2550–2562, **Crossref**

Mantyla, A. W., J. L. Reid (1983) , Abyssal characteristics of the World Ocean waters, *Deep-Sea Res., Part A*, *30*, p. 805–833, **Crossref**

Morozov, E. G. (2005) , Cruise 17 of R/V Akademik Sergei Vavilov in the Atlantic Ocean, *Oceanology*, *45*, no. 3, p. 441–443.

Morozov, E. G., A. N. Demidov, R. Yu. Tarakanov (2008) , Transport of Antarctic waters in the deep channels of the Atlantic Ocean, *Doklady Earth Sciences*, *423*, no. 8, p. 1286–1289, **Crossref**

Morozov, E. G., A. N. Demidov, R. Yu. Tarakanov, W. Zenk (2010) , *Abyssal Channels in the Atlantic Ocean: Water Structure and Flows*, 266 pp., Springer, Dordrecht, **Crossref**

Morozov, E. G., R. Yu. Tarakanov, D. I. Frey, D. G. Borisov (2018) , Currents and water structure north of the Vema Channel, *Russian Journal of Earth Sciences*, *18*, p. ES5006, **Crossref**

Morozov, E., D. . Frey, N. Diansky, V. V. Fomin (2019) , Bottom circulation in the Norwegian Sea, *Russian Journal of Earth Sciences*, *19*, p. ES2004, **Crossref**

Orsi, A. H., G. C. Johnson, J. L. Bullister (1999) , Circulation, mixing, and production of Antarctic Bottom Water, *Prog. Oceanogr.*, *43*, p. 55–109, **Crossref**

Orsi, A. H., S. S. Jacobs, A. L. Gordon, M. Visbeck (2001) , Cooling and ventilating the abyssal ocean, *Geophys. Res. Lett.*, *28*, p. 2923–2926, **Crossref**

Sandoval, F. J., G. L. Weatherly (2001) , Evolution of the Deep Western Boundary Current of Antarctic Bottom Water in the Brazil Basin, *J. Physical Oceanography*, *31*, no. 6, p. 1440–1460, **Crossref**

Sarkisyan, A. S. (1991) , *Simulation of Oceanic Dynamics*, Gidrometeoizdat, St. Petersburg (in Russian).

Zalesny, V., N. Diansky, V. Fomin, S. N. Moshonkin, S. G. Demyshev (2012) , Numerical model of the circulation of the Black Sea and the Sea of Azov, *Russ. J. Numerical Analysis Mathematical Modelling*, *27*, no. 1, p. 95–111, **Crossref**

Zalesny, V. B., G. I. Marchuk, V. I. Agoshkov, et al. (2010) , Numerical simulation of large-scale ocean circulation based on the multicomponent splitting method, *Russ. J. Numerical Analysis Mathematical Modelling*, *25*, no. 6, p. 581–609, **Crossref**

Zenk, W., N. G. Hogg (1996) , Warming trend in Antarctic Bottom Water flowing into the Brazil Basin, *Deep-Sea Res. I*, *43*, no. 9, p. 1461–1473, **Crossref**

Zweng, M. M., J. R. Reagan, J. I. Antonov, et al. , *World Ocean Atlas 2013, Vol. 2: Salinity, S. Levitus (ed.), A. Mishonov (techn. ed.)*, 39 pp., NOAA Atlas NESDIS 74, USA (http://www.nodc.noaa.gov/ OC5/indprod.html).

Warren, B. A., C. Wunsch (Eds.) (1981) , Deep circulation of the world ocean, *Evolution of Physical Oceanography, B. A. Warren and C. Wunsch (Eds.)*, p. 6–41, MIT Press, Cambridge, Mass.

Weatherall, P., K. M. Marks, M. Jakobsson, et al. (2015) , A new digital bathymetric model of the world's oceans, *Earth and*

*Space Science*, *2*, no. 8, p. 331–345, **Crossref**

Wüst, G. (1936) , *Schichtung und Zirkulation des Atlantischen Ozeans (ed. Defant A.) Wissenschaftliche Ergebnisse, Deutsche Atlantische Expedition auf dem Forschungs – und Vermessungsschiff "Meteor" 1925–1927*, Walter de Gruyter [ampersand] Co., Berlin.